atmosphere

MDPI

Article

Efficacy of the CO Tracer Technique in Partitioning Biogenic and Anthropogenic Atmospheric CO_2 Signals in the Humid Subtropical Eastern Highland Rim City of Cookeville, Tennessee

Wilson K. Gichuhi [1,*] and Lahiru P. Gamage [1,2,†]

[1] Department of Chemistry, Tennessee Tech University, Cookeville, TN 38505, USA
[2] Department of Chemistry and School of Environmental Studies, Tennessee Tech University, Cookeville, TN 38505, USA
* Correspondence: wgichuhi@tntech.edu; Tel.: +1-931-372-3499; Fax: +1-931-372-6142
† Current address: Department of Agricultural and Environmental Sciences, Tennessee State University, Nashville, TN 37209, USA.

Abstract: Accurate accounting of the partition between anthropogenic and biogenic carbon dioxide mixing ratios (CO_{2Anth} and CO_{2Bio}) in urban-based CO_2 measurements is key to developing effective emission reduction strategies since such measurements can provide an independent catalogue of local and regional CO_2 emission inventories. In an attempt to delineate the contribution of CO_{2Bio} to the overall urban CO_2 mixing ratio enhancements, carbon monoxide (CO) was utilized as a tracer, following CO_2 and CO mixing ratio measurements using a wavelength-scanned cavity ring-down spectrometer (CRDS). These measurements were performed in Cookeville, TN, (36.1628° N, 85.5016° W), a medium-sized city within the Eastern Highland Rim region of the United States. Between the years 2017 and 2019, the average seasonal wintertime CO_{2Bio} mixing ratios varied between -0.65 ± 3.44 ppm and 0.96 ± 2.66 ppm. During the springtime, the observed CO_{2Bio} signals were largely negative while the CO_{2Anth} values were generally lower than the wintertime values. The contribution of CO from the isoprene oxidation reaction with the hydroxyl radical (OH) ($CO_{isoprene}$) to the overall CO enhancement during the growing season was estimated to be ~17–27 ppb, underscoring the importance of considering the contribution of $CO_{isoprene}$ to untangling different CO_{2Anth} and CO_{2Bio} sources and sinks in high isoprene-emitting urban environments.

Keywords: biogenic carbon dioxide; cavity ring-down spectroscopy; wintertime biogenic CO_2; isoprene oxidation; Eastern Highland Rim; urban-based CO_2 measurements

Citation: Gichuhi, W.K.; Gamage, L.P. Efficacy of the CO Tracer Technique in Partitioning Biogenic and Anthropogenic Atmospheric CO_2 Signals in the Humid Subtropical Eastern Highland Rim City of Cookeville, Tennessee. *Atmosphere* **2023**, *14*, 208. https://doi.org/10.3390/atmos14020208

Academic Editors: Chinmoy Sarkar and Roger Seco

Received: 19 December 2022
Revised: 13 January 2023
Accepted: 18 January 2023
Published: 19 January 2023

1. Introduction

Although the Earth's terrestrial biosphere acts as a major sink and thereby plays a major role in reducing the accumulation of global fossil fuel carbon dioxide (CO_2) [1,2], the role played by atmospheric biospheric CO_2 in the Earth's overall carbon cycle remains poorly understood [3]. This is largely due to limitations associated with the accurate monitoring of biospheric CO_2 mixing ratio signals at global, regional, and local levels [4–7]. Both the top-down and bottom-up CO_2 monitoring approaches [8] have continued to provide detailed, up-to-date inventory data on anthropogenic emissions from different sectors such as on-road transportation, residential heating, power generation, and agricultural land use. Nevertheless, the accurate determination of the partition between the net urban biogenic and anthropogenic CO_2 sources and sinks continues to pose major challenges. One such challenge involves the quest to disentangle anthropogenic and biogenic sources and sinks of CO_2, which requires deploying expensive monitoring strategies that include radioisotope techniques [9–11] or multi-species sampling [12,13]. In the recent past, other monitoring techniques such as unmanned aerial vehicle (UAV)-based Aircore [14] and light

detection and ranging (LIDAR) [15] have been utilized as alternative monitoring methods to obtain spatial atmospheric CO_2 ratios from strong point sources with high accuracy.

Although urban areas are directly or indirectly responsible for the majority of the reported anthropogenic CO_2 emissions [16], studies involving the measurement of urban anthropogenic and biogenic CO_2 mixing ratio signals and the influence of urban vegetation on carbon flows are rather scarce, leading to many urban anthropogenic carbon emissions being poorly constrained [17–19]. Since many urban ecosystems are surrounded by vegetation, unique growing conditions in urban ecosystems facilitate elevated biospheric carbon cycling rates relative to non-urban ecosystems, leading to the urban heat island effect (UHI) [20] and an extended urban growing season [21,22]. As a result, the deployment of highly precise and accurate instruments to measure urban CO_2 mixing ratio signals is critical since accurately measured CO_2 mixing ratio signals are critical components in the derivation of net CO_2 fluxes at regional scales.

Urban near-surface CO_2 mixing ratio measurements are complicated by high spatiotemporal variability and complex atmospheric processes that govern CO_2 fluxes within the urban domains [23–25]. Nevertheless, following recent unprecedented measurements of large biogenic carbon signals supporting stronger than expected growing season photosynthetic uptake in the southeastern United States by the Atmospheric Carbon Transport (ACT)-America Earth Venture mission [12], the need to disentangle urban anthropogenic and biogenic CO_2 sources cannot be overemphasized. Indeed, recent studies in Los Angeles (LA), a megacity in the United States, have shown that even for dry urban areas dominated by transportation and industrial emissions, the accuracy of urban fossil fuel CO_2 emission signals can be hampered by a large urban biogenic CO_2 mixing ratio signal with an unexpected origin that is traced to the irrigation of turf and other urban vegetation [26].

Currently, continental and global fossil fuel CO_2 emission data are readily available from top-down inventories, with a few studies documenting biospheric CO_2 emissions [10,27]. However, despite the advancement in both top-down and bottom-up CO_2 measurement and modelling techniques, the magnitude and variability of anthropogenic and biospheric urban CO_2 mixing ratio signals remain poorly unknown and characterized in many urban cities of the world. To this end, the present study is inspired by the continued need to obtain near-surface urban CO_2 mixing ratio data that delineates biogenic CO_2 mixing ratio signals from the anthropogenic component in a humid subtropical urban climate located within the poorly characterized southern region of the United States. This, in part, is a follow-up on the Miller et al. [26] suggestion to use reliable methods to separate fossil and biogenic CO_2 signals in wetter urban areas. In our previous work [28], we utilized the CO tracer technique to evaluate near-surface emission ratios in the city of Cookeville. As a continuation of our efforts to understand and characterize near-surface CO_2 and CH_4 mixing ratios patterns within the Eastern Highland Rim region of the United States [28,29], we now utilize the CO tracer technique to partition the observed ground-based CO_2 mixing ratios into anthropogenic and biogenic components. It should be made clear that whereas CO_2 flux studies usually utilize the eddy covariance method [30] to measure gas transport and emission rates between the surface and the atmosphere by considering the respiration characteristics of soil, vegetation, and soil microorganisms, the focus of the present study is not to estimate CO_2 fluxes but to characterize the CO_2 mixing ratios within the urban boundary layer. Using the CO tracer technique, [28,31–34] the contribution of biogenic CO_2 towards the overall near-surface CO_2 mixing ratios is then estimated and compared to related studies in other urban areas [26,35].

As a caveat, careful accounting of CO sources and sinks must be carried out when utilizing the CO tracer technique since CO can have other major non-fossil fuel sources such as wildfires and the atmospheric oxidation of methane and non-methane hydrocarbons [36–38]. For example, in 2004, Hudman et al. [39] estimated that over 50% of the total CO in the eastern United States during the summertime was due to oxidation of biogenic volatile organic compounds such as isoprene. In addition to the Parazoo et al. study carried out in the southeastern region of the United States, Ref. [12], several other studies have indicated that the non-fossil fuel CO

fraction is indeed greater than the value reported in many inventories [40–43]. Based on the uncertainty and unavailability of biogenic CO data at regional and local levels, we have adopted a first-order kinetics method from Vimont et al. [44] and our previous work [28] to estimate the overall contribution of methane and isoprene to the total CO budget in Cookeville. Whereas the contribution of CH_4 + OH oxidation toward the net urban CO mixing ratio signal is estimated to be negligible, the overall CO enhancement from isoprene oxidation during the growing season is estimated to be significant enough to affect the utilization of the CO tracer technique in partitioning urban biogenic and anthropogenic CO_2 mixing ratio signals. The results from this study can be useful as a ground-truthing for the evaluation of satellite measurements and regional climate air quality models.

2. Study Site and Methods

2.1. Study Site

Figure 1A is a map showing the location of Cookeville (36.1628° N, 85.5016° W), the neighboring counties, main interstates, and state highways. The city is situated in the Eastern Highland Rim region of the United States within the larger Upper Cumberland Plateau of Tennessee, near the crossroads of Interstate 40 (I-40), State Route 136 (SR 136), and U.S. Route 70N (US 70N). The light blue arrow in Figure 1A denotes the location of Tucker Stadium (36.17823° N, 85.50693° W) where the measurements in the current study were taken. The city is one of Putnam County's micropolitan areas and is located between the two major cities of Nashville and Knoxville along I-40. As of 2020, the city had a population of about 35,000.

A)

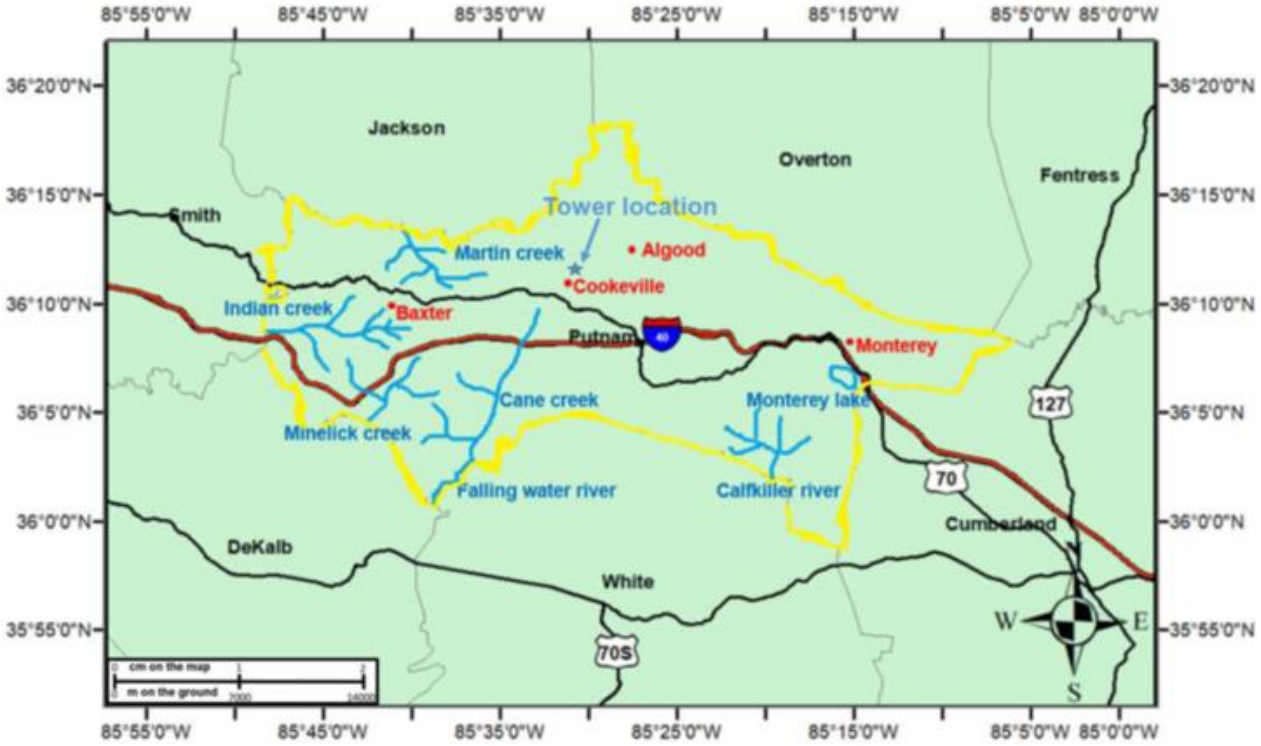

Figure 1. *Cont.*

B)

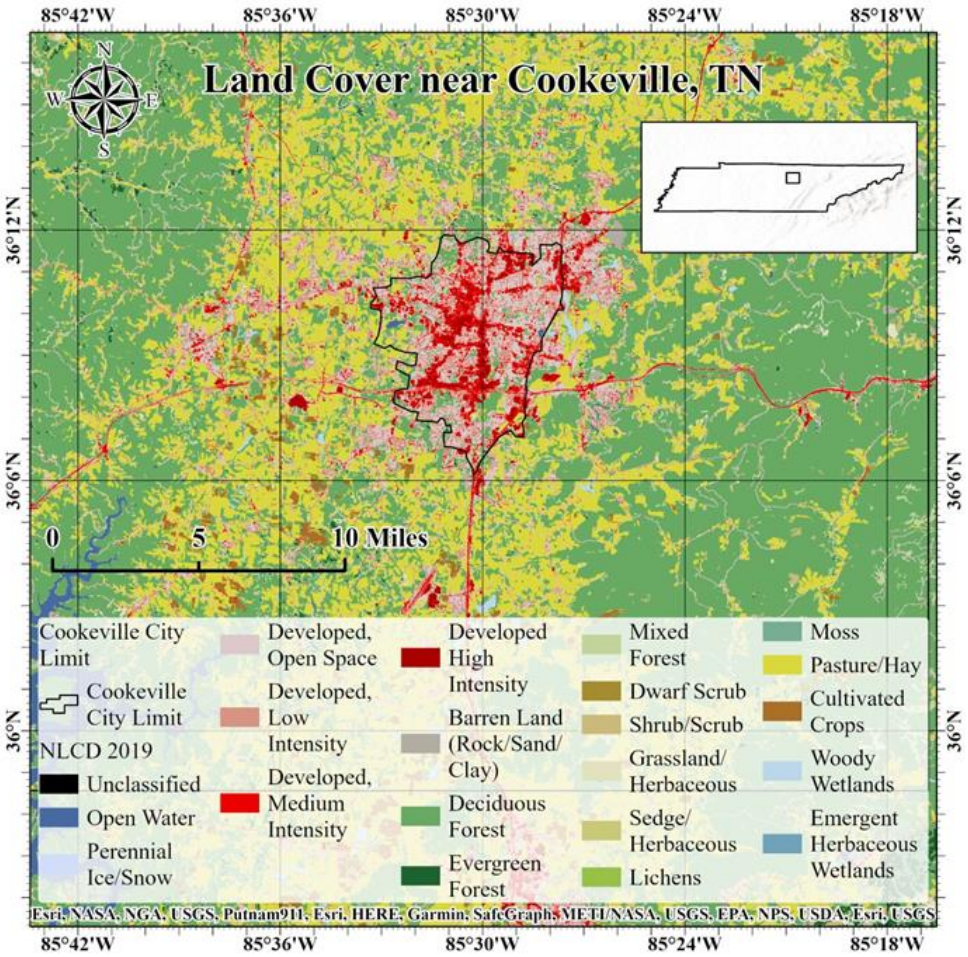

Figure 1. (**A**) Map showing the location of the measurement site (36.1628° N, 85.5016° W) and surroundings of the city of Cookeville with the neighboring counties and major highways. A detailed description of Cookeville can be found in the main text. (**B**) GIS land cover map showing detailed broadleaf and deciduous trees and shrubs for the region surrounding the Cookeville urban domain. The data used to construct the map were initially obtained from the Land Cover Database (NLCD) 2019 Products (ver. 2.0, June 2021) [45].

Cookeville has a total area of 1405 acres, with ~0.77% and ~40% of the total land being watersheds and canopy cover, respectively. In terms of climate, the city experiences relatively high temperatures and evenly distributed annual precipitation, which is typical of a humid subtropical climate. With an elevation of 1000 ft above mean sea level (AMSL), Cookeville experiences slightly lower temperatures and humidity than the Nashville Basin and the Tennessee Valley whose elevations are a few hundred feet lower. Specifically, Cookeville experiences a hot season between May and September with average daily temperatures that are above 26.7 °C. The hottest month, July, has an average high temperature of 31.1 °C and a low of 18.8 °C. The cold season in Cookeville lasts between November 27 March 1 with average daily high temperatures of below 12.8 °C. January is the coldest month of the year with an average low temperature of 2.2 °C and highs of 8.3 °C [46].

Recent studies have shown that the southeastern U.S. has large natural emissions of volatile organic compounds (VOCS) that include isoprene and monoterpenes that rival the emission fluxes observed in tropical areas [47]. Using the ^{14}C tracer technique, Miller et al. [26] showed that the urban biospheric CO_2 signal component originating from urban vegetation that includes turf and trees in the dry climate of Los Angeles (LA) has an estimated amplitude of 4.3 ppm, representing 33% of the observed annual mean fossil fuel contribution of 13 ppm [26]. The results from the Miller et al. [26] study suggest that irrigated urban

vegetation is a major contributor to the observed biospheric signal in the dry megacity of LA. Intuitively, the biospheric contribution to the overall above background CO_2 mixing ratios in other wetter and greener urban areas such as Cookeville is expected to be larger. As a result, Cookeville, a medium-sized city that is surrounded by vast vegetation, provides an ideal site to study anthropogenic–biogenic CO_2 exchange and interactions. Presented in Figure 1B is a detailed land cover map showing broadleaf and deciduous trees and shrubs for the region surrounding the city of Cookeville.

2.2. Continuous Wavelength-Scanned Cavity Ring-Down Measurements

CO_2, CO, and CH_4 dry mixing measurements were carried out using a Picarro G2401 gas concentration analyzer. The analyzer's precision at 5 s, 5 min, and 60 min is 15, 1.5, and 1 ppb for CO; 50, 20, and 10 ppb for CO_2; and 1, 0.5, and 0.3 ppb for CH_4, respectively. The maximum drift at standard temperature and pressure (STP) over 24 h is 10 ppb for CO; 100 ppb for CO_2; and 1 ppb for CH_4. The instrument is equipped with water correction software that automatically reports dry gas mole fractions. Calibration gases (from Airgas: an Air Liquide Company in the USA) were introduced to the analyzer using three whole-air, high-pressure reference gas cylinders with known CO_2 and CH_4 concentrations based on the recommended World Mereological Organization (WMO) compatibility goals of respective gases ($\pm$100 ppb and $\pm$2 ppb for CO_2 and CH_4, respectively) at 5 s, 5 min, and 1 h precision analysis test windows. Concentrations of the calibration gases spanned the expected range of atmospheric concentrations. Measurements were recorded at 5 s frequencies. All of the data used in this study were averaged from their original measurement frequency into hourly averages. Further details regarding the calibration materials, uncertainty measurements, and postprocessing of CO_2, CO, and CH_4 data used in this analysis can be found in a previous publication by Gamage et al. [28].

A manual inspection of the raw cavity ring-down spectrometer (CRDS) data was undertaken to exclude CO, CH_4, and CO_2 observations impacted by local point sources that include unusually high traffic signals, breath from the CRDS instrument operator on the sampling inlet, and agricultural- or domestic-related emissions. The obvious, significant local point sources were easily observed in the acquired ground urban mixing ratio measurements based on spikes that lasted a few seconds to a few minutes. Further data flagging and filtering was achieved by applying a two-standard deviation (2σ) filter in the observed CO, CH_4, and CO_2 mixing ratios. The total datasets subjected to the manual inspection and filtering were less than 0.5% of the entire data, with over 95% of the data being validated.

NIST traceable primary and secondary gas standards from Air Gas, an Air Liquide company based in the USA, were used to maintain calibration and the check drift and precision of the G2401 Picarro CRDS instrument. Periodically, we performed short-term drift tests (24 h and 48 h drift analysis). During the measurement period, we did not see any significant drifts or change in the calibration curve, allowing us to use the instrument for many months without any significant re-calibration. To eliminate unusually high mixing ratio signals from point sources, the instrument inlets were placed 15 m above the ground on the President's box on the west side of the Tucker football stadium at Tennessee Tech University at a flow rate of 350–400 sccm.

2.3. Estimation of Urban Biogenic and Anthropogenic CO_2 Signal

In our previous publication [28], we provided a detailed description of how the CO tracer technique can be utilized to estimate ground-based CO:CO_2 emission ratios. Here, we utilize the same model to estimate the partition of the urban CO_2 signal into anthropogenic and biogenic components for the winter and spring seasons only. According to Equation (1), the overall atmospheric CO_2 signal ($CO_{2(Tot)}$) is composed of background CO_2 (CO_{2Bg}), anthropogenic CO_2 (CO_{2An}), and the biogenic CO_2 (CO_{2Bio})

$$CO_{2_{(Tot)}} = CO_{2_{Bg}} + CO_{2_{An}} + CO_{2_{Bio}} \quad (1)$$

As a result, the biogenic CO_2 signal, CO_{2Bio}, can be calculated using Equation (2)

$$CO_{2_{Bio}} = CO_{2_{(Tot)}} - (CO_{2_{Bg}} + CO_{2_{An}}) \quad (2)$$

During the winter and early spring seasons, the overall CO ($CO_{(Tot)}$) mixing ratios can be considered as being composed of background and local/regional signals with no biogenic contribution. However, during the summertime and late springtime, an additional biogenic CO source is expected to contribute to the overall CO mixing ratio signal since the Cookeville urban domain is surrounded by leafy deciduous vegetation, a significant source of biogenic non-methane volatile organic compounds (NM-VOCs), with isoprene being the dominant contributor [48–52].

The contribution of wildfires and the burning of biomass toward the overall CO mixing ratio signal can be ruled out since no major incidents of wildfires or biomass burning were reported within the monitoring site during the study period. A similar approach of utilizing the CO as a tracer in estimating the regional biospheric CO_2 signal was adopted by Oney et al. [31]. Using this approach, the local/regional anthropogenic wintertime CO (CO_{An}) can be estimated using Equation (3), which is basically the difference between the total CO mixing ratio signal and the background CO concentrations as estimated based on the fifth-percentile subtraction procedure

$$CO_{An} = CO_{(Tot)} - CO_{Bg} \quad (3)$$

Assuming that the CO and CO_2 are co-emitted by anthropogenic sources at a given ratio, β (CO_2:CO), the anthropogenic CO_2 signal (CO_{2An}) can be derived from CO_{An} as follows:

$$CO_{2_{An}} = \beta(CO_{An}) \quad (4)$$

By combining Equation (1) through (4), we can use Equation (5) to estimate the CO_2 biogenic signal in Cookeville

$$CO_{2_{Bio}} = CO_{2_{(Tot)}} - CO_{2_{Bg}} - \left(CO_{(Tot)} - CO_{Bg}\right)\beta \quad (5)$$

The value of β (CO_{2An}:CO_{An}) is basically an emission ratio determined by the weighted least squares regression method, taking into account the uncertainties in both the measured CO_2 and CO mole fractions [53].

2.4. Review of Methane and Biogenic Isoprene's Contribution to CO in Cookeville

To utilize the CO tracer technique to partition urban CO_2 mixing ratios into anthropogenic and biogenic CO_2 components, it is worthwhile to review how biogenic emissions from VOCS might influence the overall CO budget in an area surrounded by deciduous vegetation such as Cookeville. In this section, we utilize a simple first-order kinetic model to highlight the importance of careful accounting of CO biogenic signals during the growing season when using CO as a tracer. As the predominant VOC emitted by vegetation during warm weather [54–56], the short-lived, highly reactive isoprene (C_5H_8) contributes to atmospheric reactions that control the concentrations and lifetimes of longer-lived species such as CO. As mentioned by Duncan et al., interpreting atmospheric CO concentration levels requires accurate accounting of all CO sources and sinks that include CO production from CH_4 and C_5H_8 oxidation [37] since the measured urban CO signals are part of a sequence of atmospheric photochemical reactions that involve CH_4, C_5H_8, and the OH radical. To this end, we briefly utilize a simple first-order reaction model by Vimont et al. [44] to review and estimate the respective overall effect and magnitude of CH_4 and C_5H_8 oxidation reactions on CO mixing ratios within the Cookeville city limits.

Noting that the predominant loss mechanism for atmospheric CO is the primary reaction with the OH radical, we utilize Equation (6) to calculate the effective change in CO mixing ratios resulting from the OH + CH_4 oxidation reaction

$$\Delta X_{CO} = \gamma\left(X_{CH_4,i}\right)\left[1 - e^{-k_{OH}[OH]t}\right] \quad (6)$$

ΔX_{CO} in Equation (1) is the change in CO mole fraction due to CH_4 oxidation by OH; γ is the CO yield from OH + CH_4 reaction, which in this case, is 0.96 mole of the CO produced per mole of CH_4; $\left(X_{CH_4,i}\right)$ is the measured CH_4 mole fraction (i.e., the average CH_4 mole fraction during the sampling period, which is 1900 nmol:mol); and k_{OH} is the room temperature (298 K) and pressure (1 atm) reaction rate constant for the CH_4 + OH reaction, which is 6.4×10^{-15} cm^3 s^{-1}; [57]. The OH utilized in this case corresponds to the maximum [OH] concentration in a polluted environment, which is 2×10^7 molecules cm^{-3}; and t is the theoretical transit time. For isoprene, we estimate the value of $CO_{isoprene}$ based on a transit time of 1.4 h. This transit time is the travel time between the forest edge where isoprene is produced to the urban core. Unlike the long-lived CH_4, which has an atmospheric lifetime of nearly 10 years [58] and so is relatively well-mixed in the atmosphere, isoprene is rapidly oxidized by the OH radical, especially near its source [59]. Isoprene's high reactivity limits its accumulation in the atmosphere such that, despite its large flux, only moderate mixing of up to 10 ppb is observed, mostly near its source [60]. Under typical atmospheric summer daytime conditions, the chemical conversion of isoprene into more oxidized VOCs occurs with a time constant of approximately 1 to 2 h [61,62]. At standard temperature and pressure conditions (300 K and 760 Torr), the reaction of isoprene with OH is the dominant sink [63].

Using Equation (6), we obtain a value of 0.84 nmol:mol as the maximum amount of CO produced from the oxidation of CH_4. To estimate the contribution of isoprene to the CO budget in Cookeville, we use a value of 8.9 ppb for the isoprene mixing ratio as reported by Helming et al. [64] during the Nashville Southern Oxidants Study (SOS). The Nashville SOS reported isoprene mixing ratio levels as high as 8.9 ppm in a forest site near Oak Ridge, Tennessee, with the other biogenic VOCs of α-pinene, β-pinene, and limonene having mixing ratios value close to 1 ppb [64]. We estimate the CO yield from the isoprene oxidation using values of 1.90 [63] and 3.0 [65] as the total number of CO molecules produced per molecule of isoprene. With an OH + C_5H_8 reaction rate constant of 1.0×10^{-10} cm^3 s^{-1} [62], a maximum [OH] concentration value of 2×10^7 molecules cm^{-3} [66] and a transit time of 1.4 h, we estimate the amount of CO production from isoprene oxidation ($CO_{isoprene}$) to be between 17.1 and 27.0 nmol:mol. In 2021, the Atmospheric Carbon Transport (ACT)–America Earth Venture mission reported summertime biogenic CO enrichment on the order of 40–80 ppb [12]. The stronger than expected summertime CO enrichment reported by the ACT–America airborne mission is spread mostly evenly throughout the southeastern United States and is driven by CO_2 uptake. Our estimated urban $CO_{isoprene}$ and the CO enhancements from biogenic sources reported by the ACT–America airborne mission highlights the importance of considering CO emissions from precursor greenhouse gas emissions such as NM-VOCs in any CO or CO_2 measurements within the southern part of the United States.

As the air parcel is advected from the canopy, isoprene rapidly reacts with the OH radical to form CO product. The OH radical is extremely reactive, with a lifetime of less than a second; therefore, if we assume that the OH reacts as soon as it is formed; we can use Equation (6) to calculate the maximum amount of CO produced at the forest canopy and transported to our study site by wind (using a wind speed of 4.0 miles per hour), assuming that in the canopy, the rate of production of isoprene exceeds its rate of destruction. Using a transit time of 1.4 h, we obtain a value of 27 nmol:mol as the maximum amount of $CO_{isoprene}$ that can be produced from isoprene oxidation, using 3.0 as the total number of moles of CO molecules produced per mole of isoprene. Using a CO + OH reaction rate constant of 1.44×10^{-13} cm^3 s^{-1} [62], and a transit time of 1.4 h, we estimate the loss of CO

during the transit of an air mass across Cookeville from a background measurement site using Equation (2), to obtain a ΔX_{CO} value of 1.65 nmol:mol

$$\Delta X_{CO} = (X_{CO,i}) \left[1 - e^{-k_{OH}[OH]t}\right] \quad (7)$$

Tables S1 and S2 summarize the calculated contributions to the urban CO sink and biogenic source by the respective OH + CO, OH + CH_4, and OH + C_5H_8 oxidation reactions.

3. Results and Discussion

3.1. Baseline Concentrations

To isolate the urban CO_2, CO, and CH_4 mixing ratio enhancements resulting from combustion of fossil fuels such as petroleum and natural gas within Cookeville, it is necessary to determine the baseline conditions that define background mixing ratio levels. Generally, the two main methods used by researchers to derive background CO_2 concentrations are the statistical [67,68] and the trajectory end-point methods [69–71]. In the statistical method approach, the background concentrations are based on observations only without considering atmospheric transport processes. On the other hand, the end point method uses atmospheric transport models to identify regions that are not affected by large CO_2 enhancements resulting from wildfires. To address the shortcomings associated with each of these background determination methods, Pei et al. [72] recently proposed a new Lagrangian approach that is founded on the Bayesian inversion framework.

In the present study, the baseline mixing ratio measurements are derived using the lowest fifth percentile within a three-day window centered around each hourly averaged data point to obtain a three-day running average. The baseline mixing ratios were then subtracted from the hourly averaged mixing ratio concentrations to determine the excess concentrations (i.e., "CO_{2ex}") that are due to the urban emissions of each species. It should be noted here that the baseline selected was somewhat different from the concept of a "background" concentration, which oftentimes remains unaffected by urban emissions. Figure 2 shows the monthly mixing ratio variations (solid lines) and monthly background mixing ratio values (dash lines) for CH_4 and CO_2 during the daytime (6.00 am to 6.00 pm) and the nighttime between August 2016 and July 2018. Both the CO_2 and CH_4 monthly background mixing ratios are higher during the nighttime than the daytime. The fifth-percentile background mixing ratios for CO_2, CH_4, and CO are shown in Figures S1–S3 of the Supporting Information.

3.2. Anthropogenic CO:CO_2 Emission Ratios (β^{-1} Values)

As reported in our earlier CO:CO_2 ratio study [28], in contrast to the high CO:CO_2 correlation in the wintertime, the correlations in the spring and summer are weaker [28]. In addition to the winter, spring, and summer ratios reported earlier, we also computed fall ratios. These results are summarized in Table 1. To obtain a full picture of the extent of anthropogenic emissions in the study site, we also calculated CO:CH_4 emission ratio correlations (Figure S4 and Table S3). A detailed discussion on the CO:CH_4 emission ratio correlations is provided in the Supporting Information. The summer CO:CO_2 ratios have weaker correlations mainly due to lower ground anthropogenic CO_2 mixing ratios and large, variable contributions from the strong summertime biogenic signal. The fall is a transition season that is accompanied by the foliage turning yellow or brown or dropping off. As a result, in addition to decreased photosynthesis, the biogenic signal becomes weaker in the fall season than in the summertime, leading to stronger anthropogenic CO_2 signals. The biogenic influence is dramatically reduced during the wintertime, leading to a stronger correlation above background CO_2 and CO signals since the urban CO_2 signal has a major contribution from human-induced combustion processes. The spring season is characterized by initial plant growth with greater photosynthesis than that in the winter. As a result, the springtime ratios reflect a slightly lower anthropogenic CO_2 signal than in the wintertime.

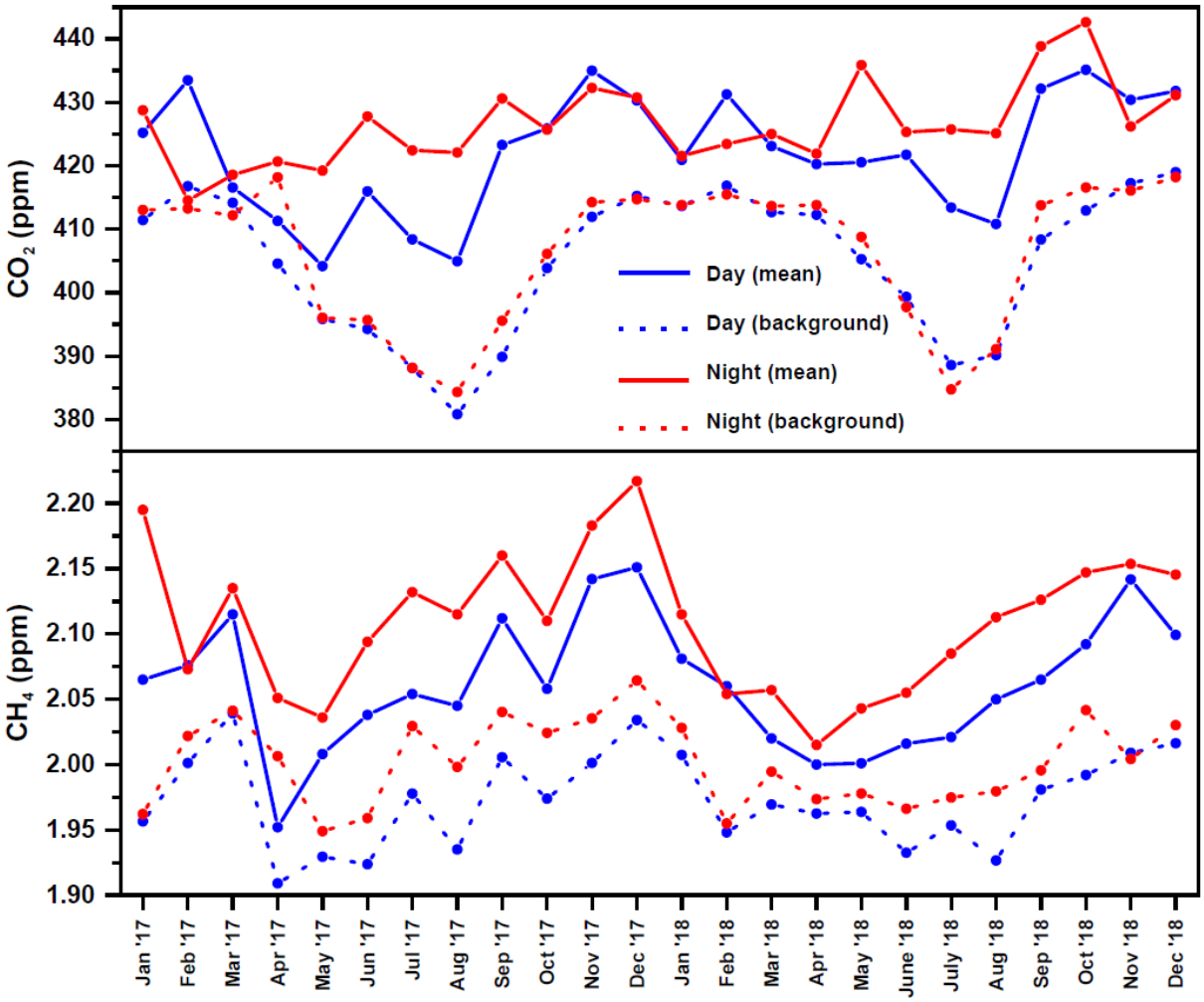

Figure 2. Daytime and nighttime mean mixing ratio values of CO_2 and CH_4. The daytime background mixing ratio values are shown in blue, and nighttime mean background values are shown in red.

Table 1. Seasonal CO:CO_2 correlation ratios (β^{-1}) in units of ppb ppm^{-1} observed between 2017 and 2019.

Year	Season	Correlation CO:CO_2 Ratio (ppb ppm^{-1})	R^2
2017	Winter	9.7 ± 0.4	0.9
	Summer	2.0 ± 0.2	0.4
	Fall	2.8 ± 0.4	0.7
	Spring	5.3 ± 0.4	0.9
2018	Winter	8.7 ± 0.5	0.8
	Summer	2.6 ± 0.5	0.4
	Fall	4.0 ± 0.4	0.8
	Spring	7.4 ± 0.7	0.7
2019	Winter	7.3 ± 0.6	0.9
	Spring	3.2 ± 0.2	0.6

3.3. Wintertime Biogenic and Anthropogenic CO_2

It is justifiable to utilize the CO tracer technique during the winter season when both the photosynthesis and respiration CO_2 signals are minimal, with CO_2 mixing ratios arising almost entirely from combustion processes. Before discussing the wintertime biogenic and anthropogenic CO_2 signals in Cookeville, we first provide a brief review

of the CO_2 mixing ratio trend in Cookeville as presented in Figure 2. Just like in other similar Northern Hemisphere urban sites [73–76], previous CO_2 mixing ratio measurements in Cookeville [28] have reported consistent diurnal and seasonal cycles that are largely influenced by atmospheric stability. The presence of strong convection that is mostly driven by both thermal heat from the Earth's surface and the turbulent shear produced by synoptic scale motion contributes to the atmospheric instability during the daytime [77].

During the night, the surface of the Earth becomes sufficiently cooled, resulting in stable nighttime atmospheric conditions that ultimately elevate CO_2 mixing ratios above the daytime levels [77,78]. Turning to the seasonal cycle, temporal differential heating of the Earth's surface by the solar radiation and varying wind speeds plays a crucial role in regulating the dynamics and stability of the atmosphere [78,79]. Weaker solar radiation and shorter daytime heating of the land's surface during the winter makes the atmosphere more stable than the springtime or summertime. As a result, the wintertime is accompanied by elevated CO_2 levels. In addition to a more unstable summertime and springtime atmosphere, increased convection and photosynthetic CO_2 drawdown during the summertime also contributes to lower CO_2 mixing ratios [80].

Although ground-based urban CO_2 measurements in Cookeville exhibit an annual cycle that is characteristic of the Northern Hemisphere, the amplitude in CO_2 mixing ratios has a larger wintertime crest than the one observed in free tropospheric global background measurement sites such as Mauna Loa, Hawaii (HI), and Niwot Ridge, Colorado [81,82]. Such differences are attributed to the influence of local to regional uptake and release processes within the urban domain. The seasonal maxima and minima occurring during the respective winter and summer months also indicate contributions from residential wintertime heating, which is superimposed on traffic and other local emission sources when photosynthesis is minimal and the diurnal atmospheric boundary layer is thinner [83].

Figure 3 shows the background-subtracted wintertime biogenic and anthropogenic CO_2 mixing ratio signals for the years 2017 through 2019. From the plot, higher variability in both the anthropogenic and biogenic signal can be seen, which correlates with diurnal variations of CO_2 mixing ratios. The average, minimum, and maximum values of anthropogenic and biogenic CO_2 mixing ratios are summarized in Table 2. From Figure 4 and Table 2, the average anthropogenic CO_2 mixing ratios between 2017 and 2019 are all positive and varied between 7.84 $\pm$ 4.33 ppm and 9.02 $\pm$ 4.46 ppm. Maximum values of 20.17 ppm, 19.94 ppm, and 15.30 ppm were recorded in the winters of 2017, 2018, and 2019, respectively. Previous measurements in the urban areas of southern Los Angeles by Fischer et al. reported anthropogenic CO_2 levels that range between 5 and 30 ppm [84]. A similar study by Newman et al., utilizing the CO tracer technique in the megacity of Los Angeles, reported overnight to midday fossil fuel CO_2 mixing ratios of 12–21 ppm, with biospheric CO_2 mixing ratios that ranged from ~2 ppm during midday to 17 ppm during the early morning [85]. Between November 2014 and March 2016, Miller et al. observed mean anthropogenic CO_2 (C_{ff}) of 14.0 $\pm$ 12.7 ppm during the winter months (November–February) in the Los Angeles megacity [26].

Turning to the wintertime biogenic mixing ratio signals, the results presented in Figure 3 and summarized in Table 2 are indicative of biogenic CO_2 mixing ratios that are largely negative. The average biogenic CO_2 mixing ratio values observed during the winters of 2017, 2018, and 2019 were 0.65 $\pm$ 3.44, 0.96 $\pm$ 2.66, and 0.17 $\pm$ 2.27 ppm, respectively. Maximum biogenic mixing ratio values that varied between 5.01 and 7.84 ppm were recorded between the years 2017 and 2019. During these three years, we observed minimum (negative) wintertime biogenic CO_2 mixing ratios that varied between -8.59 and -3.09 ppm. Similar trends where urban fossil fuel CO_2 signals are larger than biogenic signals have been observed in other urban areas such as California [84,85]. Whereas the negative biogenic mixing ratio signals indicate net CO_2 drawdown, positive biogenic values show that the contribution from respiration exceeds the one from photosynthesis. It should also be noted that just like in the study of Fischer et al. [84] we see biogenic and anthropogenic CO_2 signals that have large measurement uncertainties. The lower biogenic

signal during the wintertime is a result of reduced photosynthesis and weak plant and soil respirations [31].

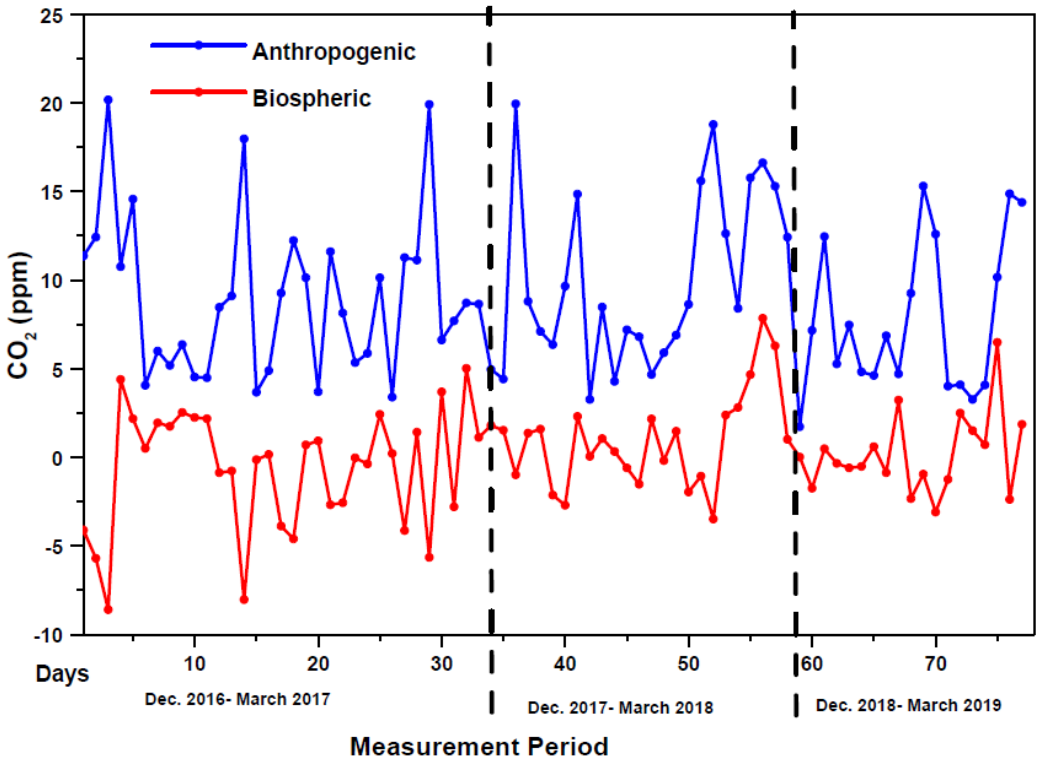

Figure 3. Wintertime biogenic and anthropogenic CO_2. The CO_2 mixing ratios in this plot were estimated using the respective wintertime β^{-1} values and Equation (5).

Table 2. Wintertime biogenic and anthropogenic CO_2 (ppm) mixing ratios calculated using the CO tracer technique. The number of days (n) in winter 2017, 2018, and 2019 are 33, 25, and 19, respectively.

	Anthropogenic			Biogenic		
Year	**Average**	**Maximum**	**Minimum**	**Average**	**Maximum**	**Minimum**
2017	9.02 ± 4.46	20.17	3.39	-0.65 ± 3.44	5.01	−8.59
2018	9.90 ± 4.94	19.94	3.26	0.96 ± 2.66	7.84	−3.48
2019	7.84 ± 4.33	15.30	1.72	0.17 ± 2.27	6.48	−3.09

To shed more light on our observed urban biogenic CO_2 signal, we compare our results with other measurements from other urban areas. Our 2017, 2018, and 2019 wintertime biogenic CO_2 mixing ratios for all of the years are mostly close to one with respective amplitudes of 4.09, 3.62, and 2.44. Wintertime and summertime enhancements of 3.5 ± 0.9 and 0.3 ± 1.0 ppm were observed in the dry metropolitan Los Angeles (L.A.) megacity in 2015 by Miller et al. [26]. Although a much more accurate $\Delta^{14}C$ tracer technique was used in the L.A. study by Miller et al. [26], we note that in addition to having a total of ~40% canopy cover that is mainly comprised deciduous trees, Cookeville has a humid subtropical climate that makes it much wetter than the dry L.A. megacity; hence, in addition to CO_{2Bio} from trees and surrounding vegetation, the biogenic CO_2 contribution from turf grass and other urban vegetation is expected to be larger than that of LA. We also note that while our seasonal CO_{2Bio} shows a significant variation as we move from wintertime to springtime, the CO_{2Bio} seasonal cycle amplitude in the L.A. megacity remains unchanged at 4.3 ppm.

3.4. Springtime and Anthropogenic CO_2

The springtime biogenic and anthropogenic CO_2 mixing ratios are presented in Figure 4 and summarized in Table 3. The average springtime anthropogenic CO_2 mixing ratios between

2017 and 2019 are all positive and varied between 5.74 ± 2.05 ppm and 8.12 ± 3.94 ppm. Maximum values of 16.68 ppm, 9.81 ppm, and 16.68 ppm were recorded in the winters of 2017, 2018, and 2019, respectively.The springtime anthopogenic CO_2 mixing ratios are slightly less than the wintertime values. This is not surprising since spring is the season when vegetation starts to appear with the the biomess transition from a net CO_2 source to a net sink.

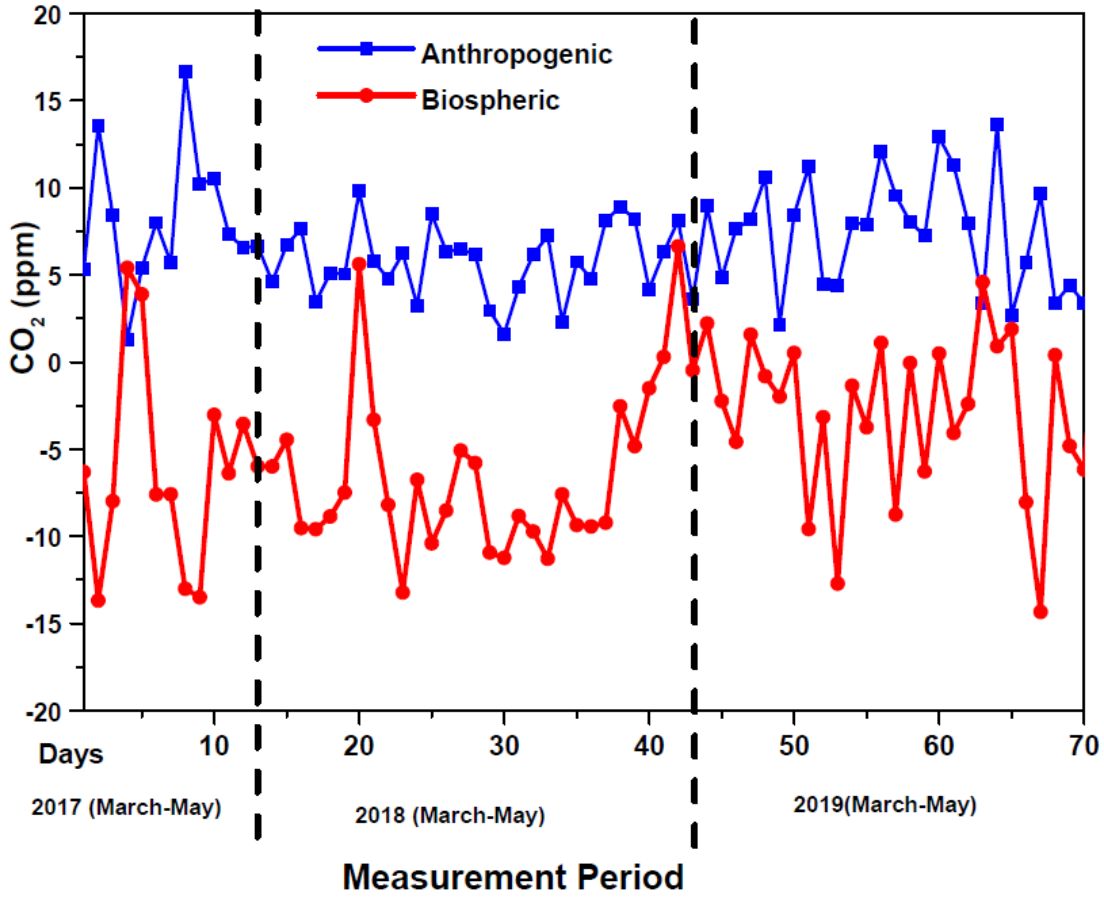

Figure 4. Springtime biogenic and anthropogenic CO_2. The CO_2 mixing ratios in this plot were estimated using the respective springtime β^{-1} values and Equation (5).

Table 3. Springtime biogenic and anthropogenic CO_2 (ppm) mixing ratios calculated using the CO tracer technique. The number of days (n) in winter 2017, 2018, and 2019 are 13, 31, and 30, respectively.

	Anthropogenic			Biogenic		
Year	**Average**	**Maximum**	**Minimum**	**Average**	**Maximum**	**Minimum**
2017	8.12 ± 3.94	16.68	1.30	−6.10 ± 5.89	5.41	−13.68
2018	5.74 ± 2.05	9.81	1.63	−6.11 ± 4.94	6.63	−13.22
2019	7.48 ± 3.22	13.65	2.14	−3.25 ± 4.65	4.58	−14.33

In contrast to the wintertime biogenic signals (Figure 3) that are close to zero, Figure 4 clearly shows that the springtime biogenic CO_2 mixing ratios are largely negative. The average biogenic CO_2 mixing ratio values observed during the spring of 2017, 2018, and 2019 were −6.10 ± 5.89, 6.11 ± 4.94, and −3.25 ± 4.65 ppm, respectively. Maximum biogenic mixing ratio values that varied between 4.58 and 5.41 ppm were recorded between the years 2017 and 2019. During the three years, we observed minimum (negative) springtime biogenic CO_2 mixing ratios that varied between −13.22 and −14.33 ppm. Although our measurements are ground-based, we now briefly compare earlier springtime boundary layer and free tropospheric aircraft measuments over the city of Sacramento, California, obtained by Turnbull et al. [35]. In the spring of 2009, Turnbull et al. measured biospheric CO_2 mixing ratios that ranged from

8 ± 2 ppm in the Sacramento urban plume to -6 ± 1 ppm in the surrounding boundary layer air [35]. Whereas photosynthesis was the main contributor to the negative biogenic CO_2 signal, Turnbull et al. [35] attributed the use of biofuels to up to 1 ppm of the observed positive CO_{2bio} signal since California required $\sim$ 8% ethanol in gasoline in 2009. The remaining positive CO_{2bio} in the Turnbull et al. study was largely attributed to agriculture and grasslands in the surrounding rural areas with trees being mentioned as the main contributor to the Sacramento urban biospheric CO_2 signal. Whereas the Sacramento measurements were taken in the springtime when biomes were transitioning from a net CO_2 source to a net sink, we note that our springtime biogenic CO_2 signal in the Cookeville urban domain is higher than the one observed in Sacramento. This is not surprising given the presence of a deeper canopy density and an urban ecology in Cookeville that is very different from that in Sacramento. The respective seasonal biogenic and anthopogenic CO_2 mixing ratios estimated using the respective wintertime and springtime β^{-1} values and Equation (5) are presented in Figure 5.

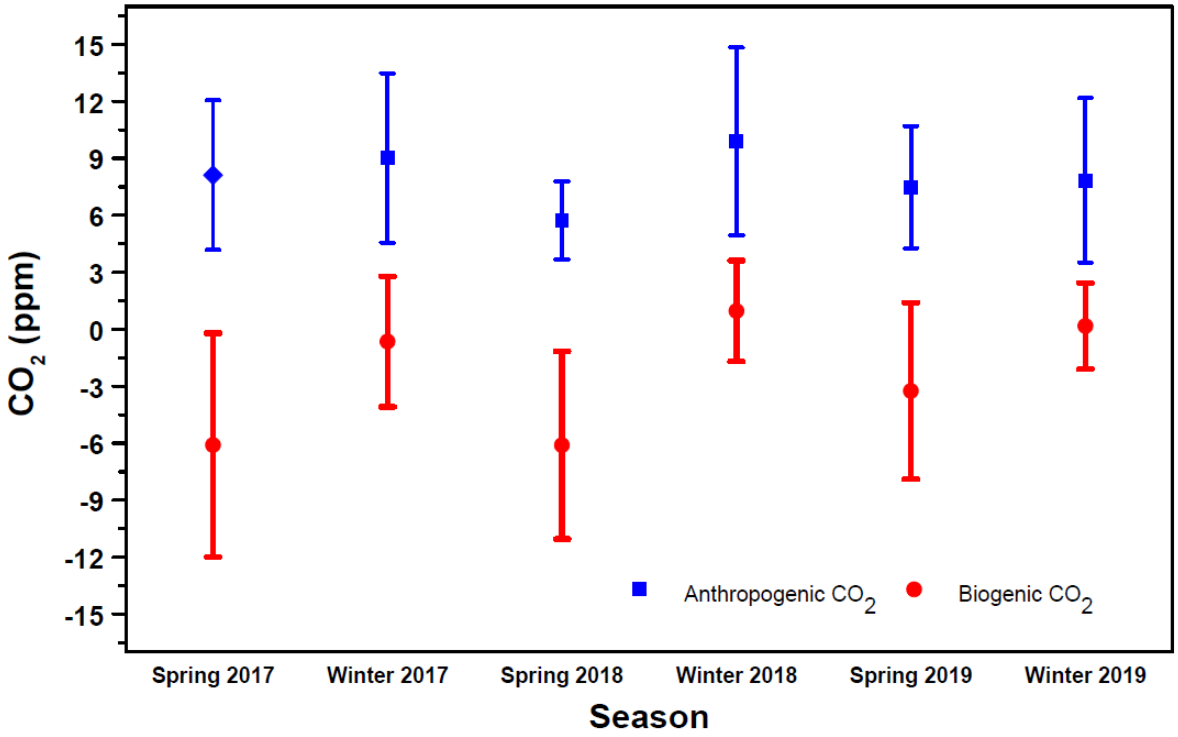

Figure 5. Seasonal wintertime and springtime biogenic (red) and anthropogenic (blue) CO_2 mixing ratios estimated using the respective wintertime and springtime β^{-1} values and Equation (5).

In summary, we have shown that for urban environments where local biogenic sources of CO are negligible, the CO tracer technique can be used to resolve the contribution of fossil-fuel-derived CO_2 to the overall CO_2 atmospheric signal. Simultaneous measurements of CO and CO_2 mixing ratios provide an avenue for obtaining continuous information about CO_2 sources, giving insights about local diurnal and seasonal patterns of energy use and respiratory fluxes. While the CO tracer technique is relatively inexpensive compared to isotopic tracer techniques [10,32], its effectiveness can be hampered by a lack of a well-defined local background and the uncertainty in the combustion efficiency of local anthropogenic CO_2 point sources.

3.5. Broader Environmental Implications: Carbon Cycle and Balance in Urban Areas

In order to achieve the ambitious goal of reducing greenhouse gas (GHG) emissions 50–52% below the 2005 levels by the year 2030 [86] and improve the current understanding of the underlying drivers of urban carbon fluxes at local and regional levels, there is a need to increase monitoring sites that acquire near-surface mixing ratio data pertaining to the contribution of biogenic CO_2 to the overall near-surface CO_2 mixing ratios. In

particular, the ultimate realization of the GHG emission reduction goal can be hampered by inadequate or a lack of accurate accounting of the sources and sinks that contribute to the overall near-surface urban CO_2 mixing ratio signals since most continuous CO_2 monitoring sites generally monitor well-mixed CO_2 mole fractions at distances far away from urban sources [87,88]. Nevertheless, in the recent past, greenhouse networks such as the Utah Urban Carbon Dioxide (UUCON) and Uintah Basin greenhouse gas networks [89] have performed extensive near-surface CO_2 campaigns where the observed CO_2 mixing ratios have not only contributed to a deeper understanding of spatial and temporal variability of emissions in urban and rural locations throughout northern Utah [90] but they have also assisted in the validation of emission inventories [91].

The present study has highlighted the importance of accurate quantification of biogenic and anthropogenic CO_2 mixing ratios in a medium-sized urban site surrounded by vast canopy cover. Despite the limited temporal coverage, studies such as the one presented in this paper have the potential to provide an independent assessment of emissions for cities. Indeed, a 2021 provocative Vulcan project reported that the average United States city has CO_2 emissions that are underestimated by nearly 20%, with some cities such as Torrance, CA, and Blacksburg, VA, reporting underestimates that were over 145% and 123% [16], respectively. The need to acquire accurate ground-based measurements of urban CO_2 mixing ratios across United States cities cannot be overemphasized. According to the latest estimates by Nowak and Greenfield [92], urban land is projected to more than double between 2010 and 2060. Such an increase in urban land is expected to have adverse impacts on forest and agricultural lands, which will in turn have a major effect on the urban CO_2 budget and air quality.

Indeed, this study has demonstrated that despite the obvious, growing dominance of anthropogenic fossil fuel emissions associated with the rapid expansion of urban areas, there is a need to take into consideration the heterogeneity of urban atmospheric CO_2 mixing ratio signals that bring about the mixing of biological and fossil fuel sources and sinks. As cities across the United States continue to set ambitious targets for reducing GHG emissions, it is of paramount importance that they keep track of how well they are meeting their decarbonization goals by counterchecking the accuracy of their CO_2 inventories with independent CO_2 measurements such as the one reported in this work. The main limitation of the current research study is the choice of background mixing ratios that may be slightly higher than the ones from a free tropospheric site. The other limitation of this study is the oversimplification of the role of CO from the oxidation of volatile organic compounds within the study area. At a time when the contribution of isoprene to the CO_2 budget is becoming more prevalent within the southeastern region of the United States, the role of biogenic CO to the overall carbon cycle should be investigated in more detail.

4. Conclusions and Future Directions

This study has provided valuable information on urban anthropogenic and biogenic CO_2 signals in Cookeville, TN, a medium-sized city located in a humid subtropical climate. Using the CO tracer technique, we obtained 2017, 2018, and 2019 wintertime biogenic CO_2 components that have amplitude values of 4.09, 3.62, and 2.44 ppm, respectively. Compared to the largely negative springtime biogenic CO_2 signals, the observed wintertime seasonal biogenic mixing ratios are positive and close to unity. The measured CO_2 signals were partitioned into anthropogenic and biogenic dry mole fractions, utilizing CO as a tracer. Between the years 2017 and 2019, the average seasonal wintertime biogenic CO_2 dry mixing ratios varied between -0.65 ± 3.44 ppm and 0.96 ± 2.66. During the three years, maximum seasonal biogenic mixing ratios that varied between 5.01 and 7.84 ppm were recorded. On the other hand, between 2017 and 2019, the average anthropogenic CO_2 mixing ratios varied between 5.74 ± 4.94 ppm and 8.12 ± 4.33 with respective maximum seasonal values of 16.68, 9.81, and 13.65 ppm. The results from this study can be useful as a ground-truthing for the evaluation of satellite measurements and regional climate air quality models. In the future, this study can be enhanced by comparing the observed anthropogenic and bio-

genic CO_2 mixing ratios to those predicted by a numerical modeling system that includes inventory-based emission estimates and atmospheric transport models. Such a comparison would be very useful in testing the degree to which the observed CO_2 mixing ratio enhancements are similar to those expected from prior knowledge of emissions and atmospheric transport. Finally, since biofuels continue to play a major role in the transport industry, the use of other tracers such as carbonyl sulfide and stable isotopes of CO_2 in future studies will improve the accuracy of the attribution of urban CO_2 signals to fossil fuel and biogenic contributions.

Supplementary Materials: The following supporting information can be downloaded at https://www.mdpi.com/article/10.3390/atmos14020208/s1. CO:CH4 Emission Ratios [40,93–103]; Figure S1. Fifth percentile CO_2 background mixing ratios (monthly averaged fifth percentile values and three-day moving average values); Figure S2. Fifth percentile CH_4 background mixing ratios (monthly averaged fifth percentile values and three-day moving average values); Figure S3. Fifth percentile CO background mixing ratios (monthly averaged fifth percentile values and three-day moving average values); Figure S4. Seasonal CO:CH_4 ratios in ppb ppm^{-1} observed between 2017 and 2019; Table S1. Estimated contributions to the urban CO sink and biogenic source by the respective OH + CO, OH + CH_4, and OH + isoprene oxidation reactions, utilizing a maximum [OH] of 2×10^7 molec./cm^3; Table S2. Estimated contributions to the urban CO sink and biogenic source by the respective OH + CO, OH + CH_4, and OH + isoprene oxidation reactions, utilizing a minimum [OH] of 1×10^6 molec./cm^3; Table S3. Seasonal CO:CH_4 ratio and correlations.

Author Contributions: Conceptualization, methodology, and writing: W.K.G.; investigation and data analysis: W.K.G. and L.P.G. All authors have read and agreed to the published version of the manuscript.

Funding: The study was funded by a Tennessee Tech Faculty starter grant and a Tennessee Tech Faculty research grant.

Institutional Review Board Statement: Not applicable.

Informed Consent Statement: Not applicable.

Data Availability Statement: The data presented in this study are contained within the article or supplementary material.

Acknowledgments: The authors wish to thank Alfred J. Kalyanapu of the Department of Civil and Environmental Engineering, Tennessee Tech University, for assistance in generating the land cover map of Cookeville. The authors also wish to thank the Department of Chemistry and the School of Environmental Sciences at Tennessee Tech for funding L.P.G. graduate studies in Environmental Science (Chemistry).

Conflicts of Interest: The authors declare no competing financial interests.

References

1. Tian, H.; Lu, C.; Ciais, P.; Michalak, A.M.; Canadell, J.G.; Saikawa, E.; Huntzinger, D.N.; Gurney, K.R.; Sitch, S.; Zhang, B.; et al. The terrestrial biosphere as a net source of greenhouse gases to the atmosphere. *Nature* **2016**, *531*, 225–228. [CrossRef] [PubMed]
2. Hes, G.; Sánchez Goñi, M.F.; Bouttes, N. Impact of terrestrial biosphere on the atmospheric CO_2 concentration across termination V. *Clim. Past* **2022**, *18*, 1429–1451. [CrossRef]
3. Keenan, T.F.; Williams, C.A. The terrestrial carbon sink. *Annu. Rev. Environ. Resour.* **2018**, *43*, 219–243. [CrossRef]
4. Marquis, M.; Tans, P. Carbon crucible. *Science* **2008**, *320*, 460–461. [CrossRef]
5. Ciais, P.; Peylin, P.; Bousquet, P. Regional biospheric carbon fluxes as inferred from atmospheric CO_2 measurements. *Ecol. Appl.* **2000**, *10*, 1574–1589. [CrossRef]
6. Kraemer, G.; Camps-Valls, G.; Reichstein, M.; Mahecha, M.D. Summarizing the state of the terrestrial biosphere in few dimensions. *Biogeosciences* **2020**, *17*, 2397–2424. [CrossRef]
7. Arneth, A.; Sitch, S.; Pongratz, J.; Stocker, B.D.; Ciais, P.; Poulter, B.; Bayer, A.D.; Bondeau, A.; Calle, L.; Chini, L.P.; et al. Historical carbon dioxide emissions caused by land-use changes are possibly larger than assumed. *Nat. Geosci.* **2017**, *10*, 79–84. [CrossRef]
8. Takata, K.; Patra, P.K.; Kotani, A.; Mori, J.; Belikov, D.; Ichii, K.; Saeki, T.; Ohta, T.; Saito, K.; Ueyama, M.; et al. Reconciliation of top-down and bottom-up CO_2 fluxes in siberian larch forest. *Environ. Res. Lett.* **2017**, *12*, 125012. [CrossRef]
9. Graven, H.; Keeling, R.F.; Rogelj, J. Changes to carbon isotopes in atmospheric CO_2 over the industrial era and into the future. *Glob. Biogeochem. Cycles* **2020**, *34*, e2019GB006170. [CrossRef]

10. Basu, S.; Lehman, S.J.; Miller, J.B.; Andrews, A.E.; Sweeney, C.; Gurney, K.R.; Xu, X.; Southon, J.; Tans, P.P. Estimating us fossil fuel CO_2 emissions from measurements of ^{14}C in atmospheric CO_2. *Proc. Natl. Acad. Sci. USA* **2020**, *117*, 13300–13307. [CrossRef]
11. Yu, M.-Y.; Lin, Y.-C.; Zhang, Y.-L. Estimation of atmospheric fossil fuel CO_2 traced by $\Delta^{14}C$: Current status and outlook. *Atmosphere* **2022**, *13*, 2131. [CrossRef]
12. Parazoo, N.C.; Bowman, K.W.; Baier, B.C.; Liu, J.; Lee, M.; Kuai, L.; Shiga, Y.; Baker, I.; Whelan, M.E.; Feng, S.; et al. Covariation of airborne biogenic tracers (CO_2, COS, and CO) supports stronger than expected growing season photosynthetic uptake in the southeastern US. *Glob. Biogeochem. Cycles* **2021**, *35*, e2021GB006956. [CrossRef]
13. Nathan, B.; Lauvaux, T.; Turnbull, J.; Gurney, K. Investigations into the use of multi-species measurements for source apportionment of the Indianapolis fossil fuel CO_2 signal. *Elem. Sci. Anth.* **2018**, *6*, 21. [CrossRef]
14. Shi, T.; Han, Z.; Han, G.; Ma, X.; Chen, H.; Andersen, T.; Mao, H.; Chen, C.; Zhang, H.; Gong, W. Retrieving CH_4-emission rates from coal mine ventilation shafts using UAV-based aircore observations and the genetic algorithm–interior point penalty function (GA-IPPF) model. *Atmos. Chem. Phys.* **2022**, *22*, 13881–13896. [CrossRef]
15. Shi, T.; Han, G.; Ma, X.; Gong, W.; Chen, W.; Liu, J.; Zhang, X.; Pei, Z.; Gou, H.; Bu, L. Quantifying CO_2 uptakes over oceans using LIDAR: A tentative experiment in bohai bay. *Geophys. Res. Lett.* **2021**, *48*, e2020GL091160. [CrossRef]
16. Gurney, K.R.; Liang, J.; Roest, G.; Song, Y.; Mueller, K.; Lauvaux, T. Under-reporting of greenhouse gas emissions in U.S. Cities. *Nat. Commun.* **2021**, *12*, 553. [CrossRef]
17. Churkina, G.; Brown, D.G.; Keoleian, G. Carbon stored in human settlements: The conterminous United States. *Glob. Chang. Biol.* **2010**, *16*, 135–143. [CrossRef]
18. Hutyra, L.R.; Duren, R.; Gurney, K.R.; Grimm, N.; Kort, E.A.; Larson, E.; Shrestha, G. Urbanization and the carbon cycle: Current capabilities and research outlook from the natural sciences perspective. *Earth's Future* **2014**, *2*, 473–495. [CrossRef]
19. Raciti, S.M.; Hutyra, L.R.; Newell, J.D. Mapping carbon storage in urban trees with multi-source remote sensing data: Relationships between biomass, land use, and demographics in boston neighborhoods. *Sci. Total Environ.* **2014**, *500–501*, 72–83. [CrossRef]
20. Yang, L.; Qian, F.; Song, D.-X.; Zheng, K.-J. Research on urban heat-island effect. *Procedia Eng.* **2016**, *169*, 11–18. [CrossRef]
21. Zhang, X.; Friedl, M.A.; Schaaf, C.B.; Strahler, A.H.; Schneider, A. The footprint of urban climates on vegetation phenology. *Geophys. Res. Lett.* **2004**, *31*, L12209. [CrossRef]
22. Melaas, E.K.; Wang, J.A.; Miller, D.L.; Friedl, M.A. Interactions between urban vegetation and surface urban heat islands: A case study in the Boston metropolitan region. *Environ. Res. Lett.* **2016**, *11*, 054020. [CrossRef]
23. Zeng, J.; Matsunaga, T.; Tan, Z.-H.; Saigusa, N.; Shirai, T.; Tang, Y.; Peng, S.; Fukuda, Y. Global terrestrial carbon fluxes of 1999-2019 estimated by upscaling eddy covariance data with a random forest. *Sci. Data* **2020**, *7*, 313. [CrossRef] [PubMed]
24. Monson, R.; Baldocchi, D. *Terrestrial Biosphere-Atmosphere Fluxes*; Cambridge University Press: Cambridge, UK, 2014; pp. 1–487.
25. Wu, D.; Lin, J.C.; Duarte, H.F.; Yadav, V.; Parazoo, N.C.; Oda, T.; Kort, E.A. A model for urban biogenic CO_2 fluxes: Solar-induced fluorescence for modeling urban biogenic fluxes (smurf v1). *Geosci. Model Dev.* **2021**, *14*, 3633–3661. [CrossRef]
26. Miller, J.B.; Lehman, S.J.; Verhulst, K.R.; Miller, C.E.; Duren, R.M.; Yadav, V.; Newman, S.; Sloop, C.D. Large and seasonally varying biospheric CO_2 fluxes in the Los Angeles megacity revealed by atmospheric radiocarbon. *Proc. Natl. Acad. Sci. USA* **2020**, *117*, 26681–26687. [CrossRef]
27. Solazzo, E.; Crippa, M.; Guizzardi, D.; Muntean, M.; Choulga, M.; Janssens-Maenhout, G. Uncertainties in the emissions database for global atmospheric research (EDGAR) emission inventory of greenhouse gases. *Atmos. Chem. Phys.* **2021**, *21*, 5655–5683. [CrossRef]
28. Gamage, L.P.; Hix, E.G.; Gichuhi, W.K. Ground-based atmospheric measurements of CO:CO_2 ratios in eastern highland rim using a CO tracer technique. *ACS Earth Space Chem.* **2020**, *4*, 558–571. [CrossRef]
29. Gamage, L.P.; Gichuhi, W.K. Efficacy of a wavelength-scanned cavity ring-down spectroscopic technique in estimating enteric methane emissions in ruminants. *ACS Earth Space Chem.* **2018**, *2*, 673–682. [CrossRef]
30. Baldocchi, D.D. Assessing the eddy covariance technique for evaluating carbon dioxide exchange rates of ecosystems: Past, present and future. *Glob. Chang. Biol.* **2003**, *9*, 479–492. [CrossRef]
31. Oney, B.; Gruber, N.; Henne, S.; Leuenberger, M.; Brunner, D. A CO-based method to determine the regional biospheric signal in atmospheric CO_2. *Tellus Ser. B* **2017**, *69*, 1353388. [CrossRef]
32. Djuricin, S.; Pataki, D.E.; Xu, X. A comparison of tracer methods for quantifying CO_2 sources in an urban region. *J. Geophys. Res. Atmos.* **2010**, *115*, D11303. [CrossRef]
33. Lopez, M.; Schmidt, M.; Delmotte, M.; Colomb, A.; Gros, V.; Janssen, C.; Lehman, S.J.; Mondelain, D.; Perrussel, O.; Ramonet, M.; et al. CO, NO_x and ^{13} CO_2 as tracers for fossil fuel CO_2: Results from a pilot study in Paris during winter 2010. *Atmos. Chem. Phys.* **2013**, *13*, 7343–7358. [CrossRef]
34. Bares, R.; Lin, J.C.; Hoch, S.W.; Baasandorj, M.; Mendoza, D.L.; Fasoli, B.; Mitchell, L.; Catharine, D.; Stephens, B.B. The wintertime covariation of CO_2 and criteria pollutants in an urban valley of the western United States. *J. Geophys. Res. Atmos.* **2018**, *123*, 2684–2703. [CrossRef]
35. Turnbull, J.C.; Karion, A.; Fischer, M.L.; Faloona, I.; Guilderson, T.; Lehman, S.J.; Miller, B.R.; Miller, J.B.; Montzka, S.; Sherwood, T.; et al. Assessment of fossil fuel carbon dioxide and other anthropogenic trace gas emissions from airborne measurements over Sacramento, California in spring 2009. *Atmos. Chem. Phys.* **2011**, *11*, 705–721. [CrossRef]

36. Faïn, X.; Rhodes, R.H.; Place, P.; Petrenko, V.V.; Fourteau, K.; Chellman, N.; Crosier, E.; McConnell, J.R.; Brook, E.J.; Blunier, T.; et al. Northern Hemisphere atmospheric history of carbon monoxide since preindustrial times reconstructed from multiple greenland ice cores. *Clim. Past* **2022**, *18*, 631–647. [CrossRef]
37. Duncan, B.N.; Logan, J.A.; Bey, I.; Megretskaia, I.A.; Yantosca, R.M.; Novelli, P.C.; Jones, N.B.; Rinsland, C.P. Global budget of CO, 1988–1997: Source estimates and validation with a global model. *J. Geophys. Res. Atmos.* **2007**, *112*, D22301. [CrossRef]
38. Gonzalez, A.; Millet, D.B.; Yu, X.; Wells, K.C.; Griffis, T.J.; Baier, B.C.; Campbell, P.C.; Choi, Y.; DiGangi, J.P.; Gvakharia, A.; et al. Fossil versus nonfossil CO sources in the U.S: New airborne constraints from ACT-america and GEM. *Geophys. Res. Lett.* **2021**, *48*, e2021GL093361. [CrossRef]
39. Hudman, R.C.; Murray, L.T.; Jacob, D.J.; Millet, D.B.; Turquety, S.; Wu, S.; Blake, D.R.; Goldstein, A.H.; Holloway, J.; Sachse, G.W. Biogenic versus anthropogenic sources of CO in the United States. *Geophys. Res. Lett.* **2008**, *35*, L04801. [CrossRef]
40. Plant, G.; Kort, E.A.; Floerchinger, C.; Gvakharia, A.; Vimont, I.; Sweeney, C. Large fugitive methane emissions from urban centers along the U.S. east coast. *Geophys. Res. Lett.* **2019**, *46*, 8500–8507. [CrossRef]
41. Müller, J.-F.; Stavrakou, T.; Bauwens, M.; George, M.; Hurtmans, D.; Coheur, P.-F.; Clerbaux, C.; Sweeney, C. Top-down CO emissions based on IASI observations and hemispheric constraints on OH levels. *Geophys. Res. Lett.* **2018**, *45*, 1621–1629. [CrossRef]
42. Kim, S.Y.; Millet, D.B.; Hu, L.; Mohr, M.J.; Griffis, T.J.; Wen, D.; Lin, J.C.; Miller, S.M.; Longo, M. Constraints on carbon monoxide emissions based on tall tower measurements in the U.S. Upper midwest. *Environ. Sci. Technol.* **2013**, *47*, 8316–8324. [CrossRef] [PubMed]
43. Salmon, O.E.; Shepson, P.B.; Ren, X.; He, H.; Hall, D.L.; Dickerson, R.R.; Stirm, B.H.; Brown, S.S.; Fibiger, D.L.; McDuffie, E.E.; et al. Top-down estimates of NO_x and CO emissions from Washington, D.C.-Baltimore during the winter campaign. *J. Geophys. Res. Atmos.* **2018**, *123*, 7705–7724. [CrossRef]
44. Vimont, I.J.; Turnbull, J.C.; Petrenko, V.V.; Place, P.F.; Sweeney, C.; Miles, N.; Richardson, S.; Vaughn, B.H.; White, J.W.C. An improved estimate for the $\delta^{13}C$ and $\delta^{18}O$ signatures of carbon monoxide produced from atmospheric oxidation of volatile organic compounds. *Atmos. Chem. Phys.* **2019**, *19*, 8547–8562. [CrossRef]
45. Dewitz, J. *National Land Cover Database (NLCD) 2019 Products*; (Ver. 2.0, June 2021); U.S. Geological Survey: Reston, Virginia, USA, 2021. [CrossRef]
46. Spark, W. Climate and Average Weather Year Round in Cookeville Tennessee, United States. Available online: https://weatherspark.com/y/15151/Average-Weather-in-Cookeville-Tennessee-United-States-Year-Round (accessed on 19 December 2022).
47. Zhang, H.; Yee, L.D.; Lee, B.H.; Curtis, M.P.; Worton, D.R.; Isaacman-VanWertz, G.; Offenberg, J.H.; Lewandowski, M.; Kleindienst, T.E.; Beaver, M.R.; et al. Monoterpenes are the largest source of summertime organic aerosol in the southeastern United States. *Proc. Natl. Acad. Sci. USA* **2018**, *115*, 2038–2043. [CrossRef]
48. Guenther, A.B.; Zimmerman, P.R.; Harley, P.C.; Monson, R.K.; Fall, R. Isoprene and monoterpene emission rate variability: Model evaluations and sensitivity analyses. *J. Geophys. Res. Atmos.* **1993**, *98*, 12609–12617. [CrossRef]
49. Pfister, G.G.; Emmons, L.K.; Hess, P.G.; Lamarque, J.-F.; Orlando, J.J.; Walters, S.; Guenther, A.; Palmer, P.I.; Lawrence, P.J. Contribution of isoprene to chemical budgets: A model tracer study with the ncar ctm mozart-4. *J. Geophys. Res. Atmos.* **2008**, *113*. [CrossRef]
50. Mao, J.; Carlton, A.; Cohen, R.C.; Brune, W.H.; Brown, S.S.; Wolfe, G.M.; Jimenez, J.L.; Pye, H.O.T.; Ng, N.L.; Xu, L.; et al. Southeast atmosphere studies: Learning from model-observation syntheses. *Atmos. Chem. Phys.* **2018**, *18*, 2615–2651. [CrossRef]
51. Goldan, P.D.; Parrish, D.D.; Kuster, W.C.; Trainer, M.; McKeen, S.A.; Holloway, J.; Jobson, B.T.; Sueper, D.T.; Fehsenfeld, F.C. Airborne measurements of isoprene, CO, and anthropogenic hydrocarbons and their implications. *J. Geophys. Res. Atmos.* **2000**, *105*, 9091–9105. [CrossRef]
52. Stroud, C.A.; Roberts, J.M.; Williams, E.J.; Hereid, D.; Angevine, W.M.; Fehsenfeld, F.C.; Wisthaler, A.; Hansel, A.; Martinez-Harder, M.; Harder, H.; et al. Nighttime isoprene trends at an urban forested site during the 1999 southern oxidant study. *J. Geophys. Res. Atmos.* **2002**, *107*, ACH 7-1–ACH 7-14. [CrossRef]
53. Krystek, M.; Anton, M. A weighted total least-squares algorithm for fitting a straight line. *Meas. Sci. Technol.* **2007**, *18*, 3438–3442. [CrossRef]
54. Sharkey, T.D.; Wiberley, A.E.; Donohue, A.R. Isoprene emission from plants: Why and how. *Ann. Bot.* **2007**, *101*, 5–18. [CrossRef] [PubMed]
55. Guenther, A.; Karl, T.; Harley, P.; Wiedinmyer, C.; Palmer, P.I.; Geron, C. Estimates of global terrestrial isoprene emissions using MEGAN (model of emissions of gases and aerosols from nature). *Atmos. Chem. Phys.* **2006**, *6*, 3181–3210. [CrossRef]
56. Levis, S.; Wiedinmyer, C.; Bonan, G.B.; Guenther, A. Simulating biogenic volatile organic compound emissions in the community climate system model. *J. Geophys. Res. Atmos.* **2003**, *108*, 4659. [CrossRef]
57. Atkinson, R. Kinetics of the gas-phase reactions of OH radicals with alkanes and cycloalkanes. *Atmos. Chem. Phys.* **2003**, *3*, 2233–2307. [CrossRef]
58. IPCC. *Climate Change 2021: The Physical Science Basis. Contribution of Working Group I to the Sixth Assessment Report of the Intergovernmental Panel on Climate Change*; IPCC: New York, NY, USA, 2021.
59. Sillman, S.; Carroll, M.A.; Thornberry, T.; Lamb, B.K.; Westberg, H.; Brune, W.H.; Faloona, I.; Tan, D.; Shepson, P.B.; Sumner, A.L.; et al. Loss of isoprene and sources of nighttime OH radicals at a rural site in the united states: Results from photochemical models. *J. Geophys. Res. Atmos.* **2002**, *107*, ACH 2-1–ACH 2-14. [CrossRef]

60. Von Kuhlmann, R.; Lawrence, M.G.; Pöschl, U.; Crutzen, P.J. Sensitivities in global scale modeling of isoprene. *Atmos. Chem. Phys.* **2004**, *4*, 1–17. [CrossRef]
61. Atkinson, R.; Arey, J. Gas-phase tropospheric chemistry of biogenic volatile organic compounds: A review. *Atmos. Environ.* **2003**, *37*, 197–219. [CrossRef]
62. Atkinson, R.; Baulch, D.L.; Cox, R.A.; Crowley, J.N.; Hampson, R.F.; Hynes, R.G.; Jenkin, M.E.; Rossi, M.J.; Troe, J.; Subcommittee, I. Evaluated kinetic and photochemical data for atmospheric chemistry: Volume II-gas phase reactions of organic species. *Atmos. Chem. Phys.* **2006**, *6*, 3625–4055. [CrossRef]
63. Bates, K.H.; Jacob, D.J. A new model mechanism for atmospheric oxidation of isoprene: Global effects on oxidants, nitrogen oxides, organic products, and secondary organic aerosol. *Atmos. Chem. Phys. Discuss.* **2019**, *19*, 9613–9640. [CrossRef]
64. Helmig, D.; Greenberg, J.; Guenther, A.; Zimmerman, P.; Geron, C. Volatile organic compounds and isoprene oxidation products at a temperate deciduous forest site. *J. Geophys. Res. Atmos.* **1998**, *103*, 22397–22414. [CrossRef]
65. Miyoshi, A.; Hatakeyama, S.; Washida, N. OH radical initiated photooxidation of isoprene: An estimate of global CO production. *J. Geophys. Res. Atmos.* **1994**, *99*, 18779–18787. [CrossRef]
66. Park, C.; Schade, G.W.; Boedeker, I. Characteristics of the flux of isoprene and its oxidation products in an urban area. *J. Geophys. Res. Atmos.* **2011**, *116*. [CrossRef]
67. Hakkarainen, J.; Ialongo, I.; Tamminen, J. Direct space-based observations of anthropogenic CO_2 emission areas from OCO-2. *Geophys. Res. Lett.* **2016**, *43*, 11–400. [CrossRef]
68. Silva, S.J.; Arellano, A.F. Characterizing regional-scale combustion using satellite retrievals of CO, NO_2 and CO_2. *Remote Sens.* **2017**, *9*, 744. [CrossRef]
69. Hu, C.; Griffis, T.J.; Lee, X.; Millet, D.B.; Chen, Z.; Baker, J.M.; Xiao, K. Top-down constraints on anthropogenic CO_2 emissions within an agricultural-urban landscape. *J. Geophys. Res. Atmos.* **2018**, *123*, 4674–4694. [CrossRef]
70. Lin, J.C.; Mallia, D.V.; Wu, D.; Stephens, B.B. How can mountaintop CO_2 observations be used to constrain regional carbon fluxes? *Atmos. Chem. Phys.* **2017**, *17*, 5561–5581. [CrossRef]
71. Houweling, S.; Aben, I.; Breon, F.M.; Chevallier, F.; Deutscher, N.; Engelen, R.; Gerbig, C.; Griffith, D.; Hungershoefer, K.; Macatangay, R.; et al. The importance of transport model uncertainties for the estimation of CO_2 sources and sinks using satellite measurements. *Atmos. Chem. Phys.* **2010**, *10*, 9981–9992. [CrossRef]
72. Pei, Z.; Han, G.; Ma, X.; Shi, T.; Gong, W. A method for estimating the background column concentration of CO_2 using the lagrangian approach. *IEEE Trans. Geosci. Remote Sens.* **2022**, *60*, 1–12. [CrossRef]
73. Lin, J.C.; Mitchell, L.; Crosman, E.; Mendoza, D.L.; Buchert, M.; Bares, R.; Fasoli, B.; Bowling, D.R.; Pataki, D.; Catharine, D.; et al. CO_2 and carbon emissions from cities: Linkages to air quality, socioeconomic activity, and stakeholders in the Salt Lake city urban area. *Bull. Am. Meteorol. Soc.* **2018**, *99*, 2325–2339. [CrossRef]
74. Churkina, G. The role of urbanization in the global carbon cycle. *Front. Ecol. Evol.* **2016**, *3*, 144. [CrossRef]
75. Pataki, D.E.; Alig, R.J.; Fung, A.S.; Golubiewski, N.E.; Kennedy, C.A.; Mcpherson, E.G.; Nowak, D.J.; Pouyat, R.V.; Romero Lankao, P. Urban ecosystems and the north american carbon cycle. *Glob. Chang. Biol.* **2006**, *12*, 2092–2102. [CrossRef]
76. Crisp, D.; Dolman, H.; Tanhua, T.; McKinley, G.A.; Hauck, J.; Bastos, A.; Sitch, S.; Eggleston, S.; Aich, V. How well do we understand the land-ocean-atmosphere carbon cycle? *Rev. Geophys.* **2022**, *60*, e2021RG000736. [CrossRef]
77. Coutts, A.M.; Beringer, J.; Tapper, N.J. Characteristics influencing the variability of urban CO_2 fluxes in melbourne, australia. *Atmos. Environ.* **2007**, *41*, 51–62. [CrossRef]
78. Stull, R.B. *An Introduction to Boundary Layer Meteorology*; Kluwer Acad.: Dordrecht, The Netherlands, 1988.
79. Golder, D. Relations among stability parameters in the surface layer. *Bound. Layer Meteorol.* **1972**, *3*, 47–58. [CrossRef]
80. IPCC. *Climate Change 2013: The Physical Science Basis. Contribution of Working Group I to the Fifth Assessment Report of the Intergovernmental Panel (IPCC) on Climate Change*; Stocker, T.F., Qin, D., Plattner, G.-K., Tignor, M., Allen, S.K., Boschung, J., Nauels, A., Xia, Y., Bex, V., Midgley, P.M., Eds.; Cambridge University Press: Cambridge, UK; New York, NY, USA, 2013; p. 1535. [CrossRef]
81. Wang, K.; Wang, Y.; Wang, X.; He, Y.; Li, X.; Keeling, R.F.; Ciais, P.; Heimann, M.; Peng, S.; Chevallier, F.; et al. Causes of slowing-down seasonal CO_2 amplitude at Mauna Loa. *Glob. Chang. Biol.* **2020**, *26*, 4462–4477. [CrossRef]
82. Sacks, W.J.; Schimel, D.S.; Monson, R.K.; Braswell, B.H. Model-data synthesis of diurnal and seasonal CO_2 fluxes at Niwot Ridge, Colorado. *Glob. Chang. Biol.* **2006**, *12*, 240–259. [CrossRef]
83. De Arellano, J.V.-G.; Gioli, B.; Miglietta, F.; Jonker, H.J.J.; Baltink, H.K.; Hutjes, R.W.A.; Holtslag, A.A.M. Entrainment process of carbon dioxide in the atmospheric boundary layer. *J. Geophys. Res. Atmos.* **2004**, *109*. [CrossRef]
84. Fischer, M.L.; Parazoo, N.; Brophy, K.; Cui, X.; Jeong, S.; Liu, J.; Keeling, R.; Taylor, T.E.; Gurney, K.; Oda, T.; et al. Simulating estimation of California fossil fuel and biosphere carbon dioxide exchanges combining in situ tower and satellite column observations. *J. Geophys. Res. Atmos.* **2017**, *122*, 3653–3671. [CrossRef]
85. Newman, S.; Jeong, S.; Fischer, M.L.; Xu, X.; Haman, C.L.; Lefer, B.; Alvarez, S.; Rappenglueck, B.; Kort, E.A.; Andrews, A.E.; et al. Diurnal tracking of anthropogenic CO_2 emissions in the Los Angeles basin megacity during spring 2010. *Atmos. Chem. Phys.* **2013**, *13*, 4359–4372. [CrossRef]
86. Bistline, J.; Abhyankar, N.; Blanford, G.; Clarke, L.; Fakhry, R.; McJeon, H.; Reilly, J.; Roney, C.; Wilson, T.; Yuan, M.; et al. Actions for reducing US emissions at least 50% by 2030. *Science* **2022**, *376*, 922–924. [CrossRef]

87. Le Quéré, C.; Raupach, M.R.; Canadell, J.G.; Marland, G.; Bopp, L.; Ciais, P.; Conway, T.J.; Doney, S.C.; Feely, R.A.; Foster, P.; et al. Trends in the sources and sinks of carbon dioxide. *Nat. Geosci.* **2009**, *2*, 831–836. [CrossRef]
88. Sun, Y.; Bian, L.; Tang, J.; Gao, Z.; Lu, C.; Schnell, R.C. CO_2 monitoring and background mole fraction at Zhongshan station, Antarctica. *Atmosphere* **2014**, *5*, 686–698. [CrossRef]
89. Bares, R.; Mitchell, L.; Fasoli, B.; Bowling, D.R.; Catharine, D.; Garcia, M.; Eng, B.; Ehleringer, J.; Lin, J.C. The Utah Urban Carbon Dioxide (UUCON) and Uintah basin greenhouse gas networks: Instrumentation, data, and measurement uncertainty. *Earth Syst. Sci. Data* **2019**, *11*, 1291–1308. [CrossRef]
90. Mitchell, L.E.; Lin, J.C.; Bowling, D.R.; Pataki, D.E.; Strong, C.; Schauer, A.J.; Bares, R.; Bush, S.E.; Stephens, B.B.; Mendoza, D.; et al. Long-term urban carbon dioxide observations reveal spatial and temporal dynamics related to urban characteristics and growth. *Proc. Natl. Acad. Sci. USA* **2018**, *115*, 2912–2917. [CrossRef] [PubMed]
91. McKain, K.; Wofsy, S.C.; Nehrkorn, T.; Eluszkiewicz, J.; Ehleringer, J.R.; Stephens, B.B. Assessment of ground-based atmospheric observations for verification of greenhouse gas emissions from an urban region. *Proc. Natl. Acad. Sci. USA* **2012**, *109*, 8423–8428. [CrossRef]
92. Nowak, D.J.; Greenfield, E.J. US urban forest statistics, values, and projections. *J. For.* **2018**, *116*, 164–177. [CrossRef]
93. Parker, R.J.; Boesch, H.; Wooster, M.J.; Moore, D.P.; Webb, A.J.; Gaveau, D.; Murdiyarso, D. Atmospheric CH_4 and CO_2 enhancements and biomass burning emission ratios derived from satellite observations of the 2015 Indonesian fire plumes. *Atmos. Chem. Phys.* **2016**, *16*, 10111–10131. [CrossRef]
94. Wong, K.W.; Fu, D.; Pongetti, T.J.; Newman, S.; Kort, E.A.; Duren, R.; Hsu, Y.K.; Miller, C.E.; Yung, Y.L.; Sander, S.P. Mapping CH_4: CO_2 ratios in Los Angeles with CLARS-FTS from mount Wilson, California. *Atmos. Chem. Phys.* **2015**, *15*, 241–252. [CrossRef]
95. Huang, W.; Xiao, W.; Zhang, M.; Wang, W.; Xu, J.; Hu, Y.; Hu, C.; Liu, S.; Lee, X. Anthropogenic CH_4 emissions in the Yangtze river delta based on a "top-down" method. *Atmosphere* **2019**, *10*, 185. [CrossRef]
96. Tohjima, Y.; Kubo, M.; Minejima, C.; Mukai, H.; Tanimoto, H.; Ganshin, A.; Maksyutov, S.; Katsumata, K.; Machida, T.; Kita, K. Temporal changes in the emissions of CH_4 and co from China estimated from CH_4/CO_2 and CO/CO_2 correlations observed at Hateruma island. *Atmos. Chem. Phys.* **2014**, *14*, 1663–1677. [CrossRef]
97. McKain, K.; Down, A.; Raciti, S.M.; Budney, J.; Hutyra, L.R.; Floerchinger, C.; Herndon, S.C.; Nehrkorn, T.; Zahniser, M.S.; Jackson, R.B.; et al. Methane emissions from natural gas infrastructure and use in the urban region of Boston, Massachusetts. *Proc. Natl. Acad. Sci. U.S.A.* **2015**, *112*, 1941–1946. [CrossRef] [PubMed]
98. Hendrick, M.F.; Ackley, R.; Sanaie-Movahed, B.; Tang, X.; Phillips, N.G. Fugitive methane emissions from leak-prone natural gas distribution infrastructure in urban environments. *Environ. Pollut.* **2016**, *213*, 710–716. [CrossRef] [PubMed]
99. Alvarez, R.A.; Pacala, S.W.; Winebrake, J.J.; Chameides, W.L.; Hamburg, S.P. Greater focus needed on methane leakage from natural gas infrastructure. *Proc. Natl. Acad. Sci. U.S.A.* **2012**, *109*, 6435–6440. [CrossRef] [PubMed]
100. Brandt, A.R.; Heath, G.A.; Kort, E.A.; O'Sullivan, F.; Pétron, G.; Jordaan, S.M.; Tans, P.; Wilcox, J.; Gopstein, A.M.; Arent, D.; et al. Methane leaks from North American natural gas systems. *Science* **2014**, *343*, 733–735. [CrossRef]
101. Brandt, A.R.; Heath, G.A.; Cooley, D. Methane leaks from natural gas systems follow extreme distributions. *Environ. Sci. Technol.* **2016**, *50*, 12512–12520. [CrossRef]
102. Ren, X.; Salmon, O.E.; Hansford, J.R.; Ahn, D.; Hall, D.; Benish, S.E.; Stratton, P.R.; He, H.; Sahu, S.; Grimes, C.; et al. Methane emissions from the Baltimore-Washington area based on airborne observations: Comparison to emissions inventories. *J. Geophys. Res. Atmos.* **2018**, *123*, 8869–8882. [CrossRef]
103. Anderson, D.C.; Lindsay, A.; DeCarlo, P.F.; Wood, E.C. Urban emissions of nitrogen oxides, carbon monoxide, and methane determined from ground-based measurements in Philadelphia. *Environ. Sci. Technol.* **2021**, *55*, 4532–4541. [CrossRef]